WILEY | Hindawi

Research Article

Ascorbic Acid 2-Phosphate-Releasing Supercritical Carbon Dioxide-Foamed Poly(L-Lactide-Co-epsilon-Caprolactone) Scaffolds Support Urothelial Cell Growth and Enhance Human Adipose-Derived Stromal Cell Proliferation and Collagen Production

Alma Kurki [1,2] **Kaarlo Paakinaho,**[1] **Markus Hannula** [1] **Jari Hyttinen** [1]
Susanna Miettinen [1,2] **and Reetta Sartoneva** [1,2,3]

[1]*Faculty of Medicine and Health Technology (MET), Tampere University, Tampere, Finland*
[2]*Research, Development and Innovation Centre, Tampere University Hospital, Tampere, Finland*
[3]*Department of Obstetrics and Gynaecology, The Hospital District of South Ostrobothnia, Seinäjoki, Finland*

Correspondence should be addressed to Alma Kurki; alma.kurki@tuni.fi

Tissue engineering can provide a novel approach for the reconstruction of large urethral defects, which currently lacks optimal repair methods. Cell-seeded scaffolds aim to prevent urethral stricture and scarring, as effective urothelium and stromal tissue regeneration is important in urethral repair. In this study, the aim was to evaluate the effect of the novel porous ascorbic acid 2-phosphate (A2P)-releasing supercritical carbon dioxide-foamed poly(L-lactide-co-ε-caprolactone) (PLCL) scaffolds (scPLCL$_{A2P}$) on the viability, proliferation, phenotype maintenance, and collagen production of human urothelial cell (hUC) and human adipose-derived stromal cell (hASC) mono- and cocultures. The scPLCL$_{A2P}$ scaffold supported hUC growth and phenotype both in monoculture and in coculture. In monocultures, the proliferation and collagen production of hASCs were significantly increased on the scPLCL$_{A2P}$ compared to scPLCL scaffolds without A2P, on which the hASCs formed nonproliferating cell clusters. Our findings suggest the A2P-releasing scPLCL$_{A2P}$ to be a promising material for urethral tissue engineering.

1. Introduction

The reconstructive surgery of urethral defects caused by urethral strictures, infections, traumas, or congenital malformations remains a great challenge [1–3]. Small defects are reconstructed with autologous genital flaps. However, larger defects require nongenital tissue grafts or allogenic grafts, in which the reconstruction is highly susceptible to complications [3–5]. Therefore, tissue engineering aims to develop new alternatives for enhanced urethral defect reconstruction. The graft material for a urethral application must be suturable, elastic, and flexible while promoting the

regeneration of the urothelium barrier and underlying smooth muscle layer and stromal tissue [6, 7].

Vast research has been conducted to discover a scaffold with adequate mechanical and bioactive properties, yet critical difficulties still remain [7, 8]. Previously, decellularized natural matrices, such as bladder acellular matrix or small intestinal submucosa, have been studied for urethral defect reconstruction [5]. Their advantage is the existence of the natural extracellular matrix (ECM) and good biocompatibility. However, the natural decellularized matrices are nontailorable, have high variability with a lack of large-scale manufacturing, and are prone to immunogenicity regardless of the

decellularization process [5, 7]. Therefore, there is an emerging interest in utilizing synthetic biodegradable polymers, such as poly-lactic acid (PLA), poly-glycolic acid (PGA), and poly-caprolactone (PCL) for urethral applications [7, 9].

The poly(l-L-lactide-co-ε-caprolactone) (PLCL), a co-polymer of PLA and PCL, has been previously studied by us and others in several soft tissue engineering applications, such as vascular and urogynaecological research [10–16]. In the PLCL copolymer, the undesired stiffness of PLA [17] and the very slow degradation time of PCL [18] can be tailored to the application's requirements. Since the urethra is a highly elastic tissue subjected to repetitive stretching and con-tracting forces, the repair material needs to enable its high flexibility and simultaneously support the urethral tubular structure for the time of the tissue regeneration [19, 20]. Therefore, as an elastic and flexible polymer, PLCL is a potential material for urethral applications [17, 21].

In addition to the biomaterial selection, the scaffold design, interconnected porosity, and pore size are highly important for the regenerating tissue. Interconnected pores serve as a route for nutrient transport and allow the mi-gration of cells and tissue in-growth into the scaffold. Moreover, the scaffold fabrication method should enable large-scale manufacturing without leaving any toxic resi-dues. Supercritical carbon dioxide ($scCO_2$)-foaming is a rapid, environmentally friendly, and cost-effective method for producing scaffolds with controlled porosity and pore size. Porosity and pore size are controlled by temperature and pressure conditions without requiring any toxic solvents or other nondesired components [22–25].

Previous preclinical studies have demonstrated that cell seeding is beneficial in urethral tissue engineering [19, 26–30]. Most importantly, the use of adipose-derived stromal/stem cells (ASCs) or smooth muscle cells has been shown to enhance angiogenesis and the formation of the urethral stromal tissue during the tissue regeneration, inhibiting the formation of urethral fibrosis [26–29]. Besides ASCs, several cell types have been utilized in urethral tissue engineering research, including fibroblasts [31, 32], smooth muscle cells [27, 33, 34], stromal/stem cells [35–38] along with urothelial cells (UCs) [10, 39–42].

As a native cell type, UCs are frequently studied for urethral tissue regeneration. It is possible to obtain UCs by performing bladder washing without the need for an in-vasive biopsy [28, 43, 44]. Still, the regeneration of the urethral stroma is highly important for the tissue-engineered urethra. Human ASCs (hASCs) are easily isolated in abundance and are demonstrated to differentiate towards smooth muscle cells [45–47]. As such, they are appealing cell alternatives to smooth muscle cells for forming urethral stromal tissue. Moreover, ASCs and other mesenchymal stem and progenitor cells are capable of reducing in-flammation and promoting angiogenesis and intrinsic tissue regeneration in situ [29, 48, 49].

Cell growth and differentiation can be aided by using bioactive molecules. Ascorbic acid (AA) is an essential nutrient and antioxidant that cannot be synthesized by human cells. It plays a central role in multiple cellular processes, such as collagen synthesis where it is a critical cofactor required to form stable collagen fibrils [50, 51]. Supplemented and scaffold-embedded AA has been dem-onstrated to increase collagen production, cell proliferation, and maturation of various cell types, such as fibroblasts, osteoblast-like cells, and hASCs [52–56]. Particularly, AA and its derivatives enhance the proliferation and differen-tiation of stem cells into several cell types, such as adipocytes, cardiac myocytes, and osteoblasts [53, 57–59]. However, AA is very unstable in aquatic conditions, so a more stable AA derivative ascorbic acid 2-phosphate (A2P) is commonly used instead [56, 60].

In this study, the aim was to reveal the potential of A2P-embedded $scCO_2$-foamed PLCL scaffold ($scPLCL_{A2P}$) for urethral tissue engineering. We studied the effects of scPLCL scaffolds with and without A2P in hUC and hASC monocultures and coculture. Human UCs were cultured to generate differentiated urothelium, and hASCs were cul-tured to initiate the formation of the urethral stroma. We hypothesized that, while supporting the growth of hUCs, the A2P embedded in $scPLCL_{A2P}$ further enhances the proliferation and collagen production of hASCs and pro-motes the formation of the urethral stromal tissue com-pared to a plain scPLCL scaffold. To our knowledge, this is the first study where either $scCO_2$-foamed or A2P-embedded scaffolds were studied for urethral applications.

2. Materials and Methods

2.1. Urothelial Cell Isolation and Culture. The hUCs were isolated from urothelium tissue pieces of three child donors, aged 3 months to 2 years 9 months during elective surgery in the Tampere University Hospital with the approval of the Ethics Committee of Pirkanmaa Hospital District, Tampere Finland (R07160) and written consent from the parents. The isolation protocol for hUCs has been presented in our previous publication [10]. Briefly, the urothelial tissue was cut into small pieces and incubated in a stripping solution of 1% HEPES (Sigma-Aldrich, St. Louis, MO, USA), 0.001% aprotinin (1 kIU/μl; Sigma-Aldrich), 0.1% EDTA (Sigma-Aldrich), and antibiotics (100 U/ml penicillin and 0.1 mg/ml streptomycin, P/S; Lonza, Bio Whittaker, Verviers, Belgium) in HBSS without Ca^{2+} and Mg^{2+} (Invitrogen, Thermo Fisher Scientific, Waltham, MA, USA) overnight at +4°C to loosen the urothelial layer. The urothelium was separated from the stroma and incubated at +37°C water bath for 30 min in 0.1% trypsin solution. The isolated hUCs were suspended in EpiLife culture medium (Gibco by Life Sciences, Thermo Fisher Scientific), supplemented with EpiLife Defined Growth Supplement (EDGS; Gibco by Life Sciences), 0.1% $CaCl_2$ (Gibco by Life Sciences) and 0.35% P/S, and cultured on CellBIND T75 flasks (Corning, Sigma-Aldrich) at 37°C in a humified atmosphere of 5% CO_2. The hUCs used in monoculture experiments were passage 4 (P4) whereas hUCs in coculture experiments were P5.

2.2. Adipose-Derived Stromal Cell Isolation and Culture. The hASC were obtained during routine elective surgery in the Tampere University Hospital from three donors, aged

between 43 and 71 years, with the approval of the ethics committee of Pirkanmaa Hospital District, Tampere Finland (R15161) and written consent from the donors. The hASCs were isolated as described previously [61, 62]. Briefly, adipose tissue was cut into small pieces and incubated on a shaker in a 37°C water bath for 1 h in 1.5 mg/ml collagenase type I solution. Digested cells were centrifuged and suspended in basic medium (BM) composed of 5% sterile filtered human serum (Biowest, Nuaillé, France) and 1% P/S (Lonza) in Minimum Essential Medium Eagle-Alpha Modification (αMEM; Gibco by Life Technologies). The cell suspension was filtered and cultured in Nunc T175 flasks (Nunc, Thermo Fischer Scientific) at 37°C in a humified atmosphere of 5% CO_2. The expression of surface proteins can be found in Table 1. The expression of surface proteins was assessed after the isolation process in passage 1 ($P1$) to ensure the quality of the isolation protocol and confirming that the isolated cells can be stated as ASCs [63, 64]. The hASCs in monoculture experiments were $P4$ and in coculture $P5$.

2.3. Scaffold Manufacturing.
The scaffold manufacturing process was similar to a previously published protocol [65]. Briefly, the porous scPLCL$_{A2P}$ scaffolds were manufactured by melt-mixing 8 wt-% of A2P (Sigma-Aldrich Chemie Gmbh, Steinheim, Germany) to PLCL 70L/30CL (PLCL 7015, Corbion Purac BV, Gorinchem, The Netherlands) in a twin-screw extrusion process, after which the material was foamed by scCO$_2$ (Waters Operating Corporation, Milford, MA, USA) using high pressure and temperature of 90°C. Porous scPLCL scaffolds were manufactured similarly but without the melt mixing of A2P. To acquire the scaffolds, the foamed rods were cut into 8 mm diameter discs with a thickness of 3-3.5 mm. The scaffolds were gamma-irradiated prior to cell culture.

2.4. Scaffold's Porosity and Assessment with X-ray Microcomputed Tomography Imaging.
The scPLCL and scPLCL$_{A2P}$ scaffolds ($n = 3$) were analysed with X-ray microtomography. MicroXCT-400 (Carl Zeiss X-ray Microscopy, Inc., Pleasanton, CA, USA) device was used with the X-ray tube voltage of 60 kV and a current of 167 μA. 1601 projections were taken with 1 sec exposure time. The pixel size was 5.64 μm. Acquired projection data were reconstructed with Zeiss' XMReconstructor software. For the pore analysis, a $3.8 \times 3.8 \times 1.2$ mm volume was selected from each scaffold. The image processing and the visualizations were made with the Avizo 3D 2021.2 software (Thermo Fisher Scientific, Waltham, MA, USA). The material of the scaffold visible in the images and denser A2P particles were segmented with manual thresholding. The interconnectivity of the scaffold pores was evaluated with a Matlab program that uses the pore size data calculated with the BoneJ plugin [66] providing size distribution of the interconnected pores. The analysis procedure is described in more detail in [67]. For accuracy, a minimum particle size of 11.28 μm (twice the used pixel size of 5.64 μm) was used for interconnectivity and A2P-particle size calculations.

2.5. Cell Seeding on Scaffolds.
Before cell seeding, the scaffolds were prewetted in culture medium, EpiLife for hUCs, and BM for hASCs, for 24 h at +37°C. The prewetted scaffolds were placed into 24-well plates for the cell experiments. For the monoculture study, 150 000 hUCs or hASCs were seeded on the surface of the scaffold in a plating volume of 50 μl. The cells were left to adhere in +37°C incubator for 2 h before adding 1 ml medium to each well. For the coculture experiment, 150 000 hASCs in 50 μl of medium were seeded on the other side of the scaffold and precultured for five days in BM to allow cell expansion. Thereafter, 150 000 hUCs in 50 μl of medium were seeded on the opposite side of the scaffold, and the medium was switched to EpiLife medium for the coculture. A visualization of the research timeline is presented in Figure 1. The cell-seeded scaffolds were cultured in a humidified +37°C incubator, and the medium was changed three times a week until analysis. The analyses were performed at d1, d7, and d14 time points.

2.6. Cell Viability and Proliferation.
Cell viability in monocultures and coculture was determined at d1, d7, and d14 time points with qualitative live/dead fluorescent staining (Invitrogen, Life Technologies) as described previously [10]. Briefly, the samples were incubated in $3.75 * 10^{-5} \mu$M ethidium homodimer-1 (EthD-1) and 0.5 μM calcein acetoxymethyl ester (Calcein-AM) solution for 1 h in RT. Unseeded scaffolds were used as negative controls. Samples were imaged with a fluorescence microscope (Olympus IX51S8F-2; camera DP71), and the images were processed with Adobe Photoshop 2022-software by adjusting contrast and brightness.

On d1, d7, and d14 time points, the relative cell number in hUC and hASC monocultures was assessed with a quantitative CyQUANT Cell Proliferation Assay kit (Invitrogen, Life Technologies). The assay was repeated with three donor lines for each cell type with three parallel samples using technical triplicates in the assay run ($n = 27$). To lyse the cells, 0.1% Triton x-100 (Sigma-Aldrich) in DPBS was added to each sample, and the lysates were stored at −70°C. For analysis, CyQUANT GR dye and lysis buffer were added to the thawed lysates, and fluorescence at 480/520 nm wavelength was measured with a Wallac Victor microplate reader (PerkinElmer Life and Analytical Sciences, Wallac, Turku, Finland). Cell numbers were calculated relative to the scPLCL d1 sample.

2.7. Scanning Electron Microscopy.
Scanning electron microscopy (SEM) was used to assess the cell attachment and morphology after 1, 7, and 14 d of cell culture in hUC and hASC monocultures using one donor line from each cell type. Samples were fixed with 5% glutaraldehyde (Sigma-Aldrich) in 0.1 M phosphate buffer (pH 7.4; Sigma-Aldrich) for 48 h at RT. The sample drying procedure with hexamethyldisilazane (HMDS; Sigma-Aldrich) was performed as described by Sartoneva et al. [68]. Samples were dehydrated with increasing series of ethanol (Altia Oyj,

Table 1: Expression of cell surface markers on the used hASC donor cell lines after isolation in passage 1 ($P1$).

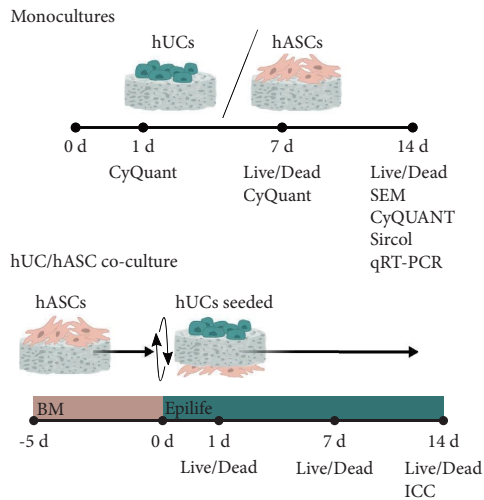| Donor line	P	Cell surface marker expression (%)							
		CD14	CD19	CD34	CD45	CD73	CD90	CD105	HLA-DR
hASC 1	1	1.2	0.6	66.7	2	99	99.7	99.7	0.6
hASC 2	1	0.3	0.2	3.7	4.1	81.4	99.2	96.3	0.4
hASC 3	1	1.1	0.8	26.7	1.5	96	98	99.7	1.8

Figure 1: Research timeline for hUC and hASC monocultures and hUC/hASC coculture. The hUC and hASC monocultures were treated similarly. In coculture, the hASCs were seeded in basic medium (BM) five days prior to seeding the hUCs on the opposite side of the scaffold and changing the coculture medium to EpiLife. The time points for mono- and cocultures were d1, d7, and d14.

Helsinki, Finland) concentrations (30, 50, 70, 80, 90, 95, and 100%) after which samples were dried with ascending series of HMDS in 100% ethanol (1 : 2, 2 : 1 and twice 100% HMDS). After HMDS was evaporated, samples were carbon sputtered and imaged with SEM (Zeiss ULTRA-plus, Oberkochen, Germany).

2.8. Total Collagen Content. Sircol soluble collagen assay (Biocolor, Carrickfergus, UK) was used to quantify the amount of total soluble collagen in hUC and hASC monocultures at d14 time point. The analysis was performed for three donor lines with three parallel samples and two technical replicates for each cell type ($n = 18$). The assay was carried out as described previously [69]. The samples were incubated in ice-cold 0.1 mg/ml pepsin (Sigma-Aldrich) in 0.5 M acetic acid for 4 h at +4°C to extract the acid-soluble collagen. Sample suspensions were moved to separate tubes, and Sircol dye reagent, consisting of picric acid and Sirius red, was added to each sample. After 30 min incubation at RT, the samples were pelleted and resuspended to ice-cold Sircol Acid-Salt Wash Reagent to remove any unbound dye. 0.5 M sodium hydroxide solution was then added to resolubilize dyed collagen. Dye intensity was measured with a Wallac Victor microplate reader at 540 nm wavelength.

2.9. Quantitative Real-Time Polymerase Chain Reaction. Quantitative real-time polymerase chain reaction (qRT-PCR) was used to analyse the relative expression of cytokeratin (CK) 7, CK8, CK19, uroplakin (UP) Ia, and UPIb in hUCs and relative expression of collagen type I (COL I), COL III, α-smooth muscle actin (αSMA), and elastin in hASCs. The assay protocol is described in more detail in [70]. For each donor line, cells from three parallel sample wells were pooled for mRNA isolation. Briefly, total RNA was isolated after 14 d of cell culturing with the NucleSpin RNA II purification kit by following the manufacturer's protocol (Macherey-Nagel GmbH & Co. KG, Düren, Germany). Isolated total RNA was then reverse transcribed to cDNA using High-Capacity cDNA Reverse Transcriptase Kit (Applied Biosystems, Foster City, CA). For the qPCR run, 50 ng of sample cDNA was added to the mixture of Power SYBR Green PCR Master Mix (Thermo Fisher Scientific) and 360 nM forward and reverse primers. Each sample was run in duplicates ($n = 6$). Used primers are listed in Table 2. The qRT-PCR run was performed using the ABI PRISM 7300 sequence detection system (Applied Biosystems). Acquired data were normalized to housekeeping gene human ribosomal protein lateral stalk subunit P0 (hRPLP0), and the relative amount of mRNA was calculated using a previously described mathematical model [71]. The ratio of hASC COL I/III mRNA was determined by using the qRT-PCR cycle threshold (Ct) values for COL I and COL III mRNA.

2.10. Cytochemical and Immunofluorescent Staining of Cocultures. Cytochemistry and immunofluorescence staining of acidic and basic cytokeratins detected in epithelial cells (mouse cytokeratin pan type I/II antibody cocktail, MA5-13156, 1 : 250; Thermo Fisher Scientific), UPIII (rabbit anti-UPK3A; orb248591, 1 : 100; Biorbyt, Cambridge, United Kingdom), and F-actin cytoskeleton organization (phalloidin-tetramethylrhodamine B isothiocyanate, P1951, 1 : 500; Sigma-Aldrich) were performed for cocultures at d14 time point ($n = 2$). Samples were fixed with 0.2% Triton x-100 (Sigma-Aldrich) in 4% PFA (Sigma-Aldrich) and incubated overnight at +4°C with primary antibodies. Secondary antibodies and phalloidin were added the next day and incubated for 45 min at +4°C. A mixture of Alexa 488 goat anti-mouse IgG1 (A21121, 1 : 400 green fluorescence; Thermo Fisher Scientific) and phalloidin was used for pancytokeratin and F-actin costaining. Alexa 594 goat anti-rabbit IgG (A11037, 1 : 300, red fluorescence; Thermo Fisher Scientific) was used for UPIII staining. Cell nuclei were stained with DAPI (1 : 2000, blue fluorescence;

Table 2: Primer sequences used in qRT-PCR assay.

Name	Primer	Sequence 5′-3′	Product size (bp)	Accession number
CK7	F	CAT CGA GAT CGC CAC CTA CC	80	NM_005556.3
	R	TAT TCA CGG CTC CCA CTC CA		
CK8	F	CCA TGC CTC CAG CTA CAA AAC	68	M34225.1
	R	AGC TGA GGT TTT ATT TTG GGA CC		
CK19	F	ACT ACA CGA CCA TCC AGG AC	80	NM_002276.4
	R	GTC GAT CTG CAG GAC AAT CC		
UPIa	F	GGG ATC TCC AGT TGT GGT GG	80	NM_007000.3
	R	TCT CAG CAA ACA GGG ACA GG		
UPIb	F	AGT CAC CAA AAC CTG GGA CAG	64	NM_006952.3
	R	TGA TGG ACC ATT TAC GCC ACA		
RPLP0	F	AAT CTC CAG GGG CAC CATT	70	NM_001002
	R	CGC TGG CTC CCA CTT TGT		
αSMA	F	GAC AAT GGC TCT GGG CTC TGT AA	194	NM_001613.4
	R	ATG CCA TGT TCT ATC GGG TAC TT		
Elastin	F	GGT GCG GTG GTT CCT CAG CCT GG	613	NM_000501.4
	R	GGG CCT TGA GAT ACC CCA GTG		
COL I	F	CCA GAA GAA CTG GTA CAT CAG CAA	94	NM_000088.3
	R	CGC CAT ACT CGA ACT GGA ATC		
COL III	F	CAG CGG TTC TCC AGG CAA GG	179	NM_000090
	R	CTC CAG TGA TCC CAG CAA TCCC		

Sigma-Aldrich). Monocultures of hUCs and hASCs cultured in EpiLife medium on polystyrene well bottom served as control samples. Cell-seeded scaffolds without primary antibodies and nonseeded scaffolds were used to exclude any nonspecific staining of the secondary antibodies or false staining caused by the scaffold material, respectively. Samples were imaged with a fluorescent microscope (Olympus IX51), and images were processed with Adobe Photoshop 2022 software by adjusting contrast and brightness.

2.11. Statistical Analysis.

Quantitative results were analysed with IBM SPSS Statistics software (Version 26, IBM Corp., Armonk, USA) using statistical tests depending on the number of samples. Mann-Whitney test or Kruskall-Wallis test for nonnormally distributed data was used for Sircol assay results ($n = 18$), CyQUANT ($n = 18$–27) and qRT-PCR results ($n = 6$). Bonferroni post hoc tests were included. Significance level $p < 0.05$ was considered as significant. All quantitative assays were performed for three donor lines for each cell type, and results from technical replicates of each sample were used in the calculations and statistical tests.

3. Results

3.1. Both scPLCL$_{A2P}$ and scPLCL Scaffolds Present High Porosity with High Interconnectivity.

Micro-CT was used to assess scaffold architecture and pore interconnectivity. In addition, the distribution of A2P particles in the scPLCL$_{A2P}$ was measured. Overall visualization of the scPLCL$_{A2P}$ and scPLCL scaffolds is represented in Figure 2. The image-based assessment revealed that the A2P particles are evenly distributed in scPLCL$_{A2P}$ (Figure 2(c)). Particles larger than $11.28\,\mu m$ were measured, and approximately 60% of A2P particles had a diameter between 11.28–$15\,\mu m$.

Average porosity was slightly lower in scPLCL$_{A2P}$ (63%) than in scPLCL (69%), yet the average pore size was higher in scPLCL$_{A2P}$ ($490 \pm 200\,\mu m$) than in scPLCL ($400 \pm 140\,\mu m$) (Table 3). In Figure 3, open porosity (y-axis) represents the percentage of interconnected scaffold pores that could be passed through by various sizes of spherical particles (x-axis) from outside of the scaffold. For example, particles with diameter $\leq 205\,\mu m$ can pass through 90% of the pores in both scPLCL$_{A2P}$ and scPLCL scaffolds (Figure 3(a)). One noticeably differing scPLCL$_{A2P}$ scaffold has been removed from the results.

3.2. A2P in scPLCL$_{A2P}$ Supports hUC and hASC Viability.

Cell viability was evaluated with Live/Dead staining on d1, d7, and d14 for monocultures and cocultures. Both hUCs and hASCs remained viable during the 14-d assessment period in monocultures. No differences were detected in hUC viability on scPLCL$_{A2P}$ and scPLCL (Figure 4). The hASCs spread rapidly on scPLCL$_{A2P}$ and covered the whole scaffold surface after 7 d, continuing to form dense cultures between d7 and d14 (Figure 5). On scPLCL, the hASCs did not spread widely along the scaffold surface but rather formed viable cell clusters during the 14-d cell culture.

Closer inspection of the monocultures with SEM on d1, d7, and d14 shows more detailed differences in the cell attachment and morphology on different scaffolds. The hUCs cultured on both scPLCL$_{A2P}$ and scPLCL presented a typical urothelial morphology with defined cell borders, and the hUCs spread evenly on scaffold surface (Figure 6). On d14, hUCs on scPLCL$_{A2P}$ had more cuboidal morphology with visible cell borders, and some hUCs had acquired apical irregularities. Instead, the hUCs on scPLCL had flattened appearance along the material surface. Uniform and aligned sheet of hASC covered the scPLCL$_{A2P}$ scaffold surface, whereas on scPLCL, the hASCs were clustered together, supporting the findings of the hASC monoculture Live/Dead viability assay (Figure 7).

According to the Live/Dead staining of hUC/hASC coculture, no distinctive difference was detected in the hUC viability and spreading between the scPLCL$_{A2P}$ and scPLCL scaffolds (Figure 8), whereas more hASCs appear to be visible on scPLCL$_{A2P}$ scaffold. After commencing coculture in Epilife medium, hASC growth on scPLCL$_{A2P}$ seems to have suppressed, yet the cells remain viable. Meanwhile, the hASCs on scPLCL formed cell clusters similar to monoculture, and after switching to Epilife medium, there seems to be more dead cells compared to scPLCL$_{A2P}$.

3.3. scPLCL$_{A2P}$ Significantly Increased the Proliferation of hASCs.

The cell proliferation of hUCs ($n = 18$–27) and hASCs ($n = 27$) on scPLCL$_{A2P}$ and scPLCL was assessed with CyQUANT by measuring the relative amount of DNA in the samples at d1, d7, and d14 time points (Figure 9). The number of hUCs was lower on scPLCL$_{A2P}$ than on scPLCL at each time point (d1 $p < 0.001$, d7 $p < 0.001$, and d14 $p = 0.009$). The number of hUCs increased between d1, d7 ($p = 0.022$), and d1–d14 ($p = 0.001$). On scPLCL, hUC number increased d1–d7 and d1–d14 ($p < 0.001$). No statistical significance in hUC amount between d7–d14 was detected on either scaffold. The number of hASCs was significantly higher ($p < 0.001$) on scPLCL$_{A2P}$ compared to scPLCL at d7 and d14 time points. Furthermore, as a function of time, the hASC proliferation on scPLCL$_{A2P}$ increased significantly from d1 to d7 ($p < 0.001$), from d1 to d14 ($p < 0.001$), and between d7 and d14 ($p = 0.003$). The cell number of hASCs on scPLCL increased between d1 and d7 ($p = 0.002$) and from d1 to d14 ($p < 0.001$). No significant increase in hASC number on scPLCL was detected between d7 and d14 ($p = 0.27$).

3.4. Collagen Production by hASCs Significantly Increased on scPLCL$_{A2P}$.

The total acid- and pepsin-soluble collagen content of samples was measured with Sircol collagen assay after 14 d of cell culture (Figure 10). Total amount of collagen in hUC monoculture ($n = 18$) was significantly lower ($p < 0.001$) on scPLCL$_{A2P}$ ($7.3 \pm 6.3\,\mu g/ml$) than on scPLCL ($26.9 \pm 4.5\,\mu g/ml$) whereas the hASCs ($n = 18$) cultured on scPLCL$_{A2P}$ produced significantly more collagen ($129.4 \pm 19.9\,\mu g/ml$, $p < 0.001$) compared to scPLCL ($49.6 \pm 14.2\,\mu g/ml$). The hASCs on scPLCL$_{A2P}$ produced approximately 17 times more collagen than hUCs. However,

(a)

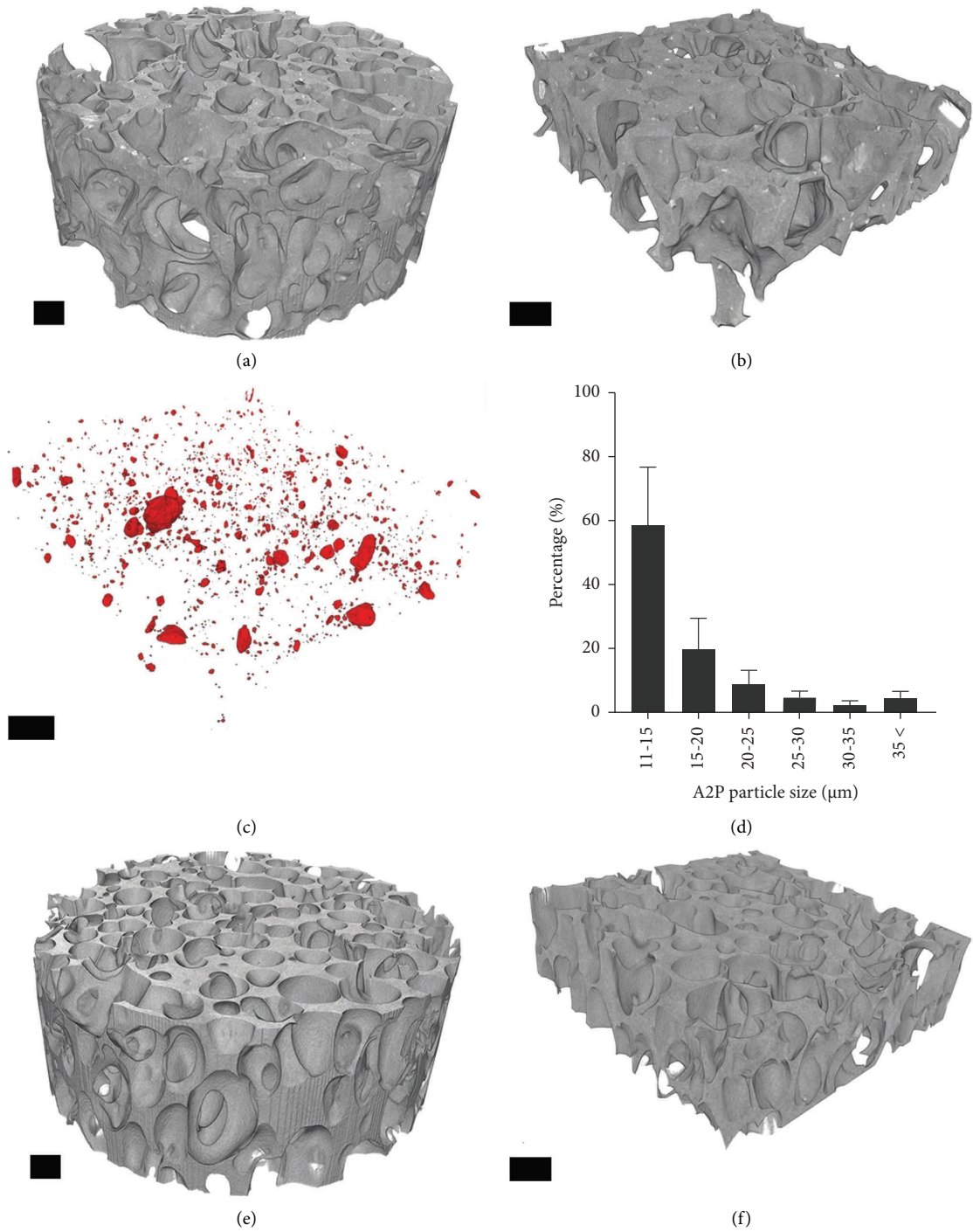
(b)

(c)

(d)

(e)

(f)

FIGURE 2: Micro-CT images of the scPLCL$_{A2P}$ and scPLCL scaffolds. Overall structure of scPLCL$_{A2P}$ scaffolds (a), volume ($3.8 \times 3.8 \times 1.2$ mm) of scPLCL$_{A2P}$ used in the porosity and A2P particle distribution measurements (b), distribution of the A2P particles in scPLCLas (c), particle size distribution ($n = 3$) (d), overall structure of scPLCL scaffolds (e), and volume ($3.8 \times 3.8 \times 1.2$ mm) of scPLCL used in the porosity measurements (f). Scale bar 500 μm.

TABLE 3: Average scaffold porosity and pore sizes ($n = 2$-3).

	Average porosity (%)	Average pore size	Maximum pore size (μm)
scPLCL$_{A2P}$	63	$490 \pm 200\,\mu$m	840
scPLCL	69	$400 \pm 140\,\mu$m	1060

(a)

(b)

(c)
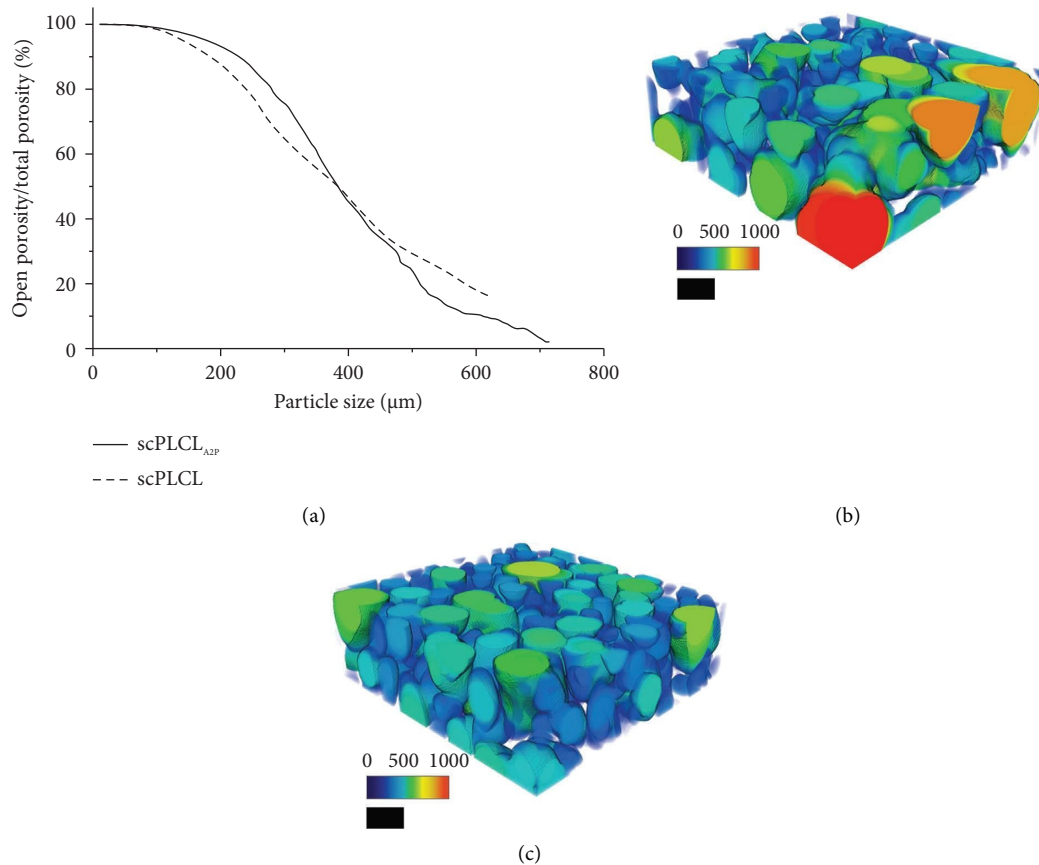
FIGURE 3: Micro-CT analysis of the scaffold pore sizes and interconnectivity. (a) Scaffold pore interconnectivity as a function of particle size capable of passing through the interconnected pores entering from outside of the scaffold. Distribution of pore sizes in scPLCL$_{A2P}$ (b) and scPLCL (c). Color scale represents the size of a particle capable of entering a pore (0–1000 μm). Scale bar 500 μm.
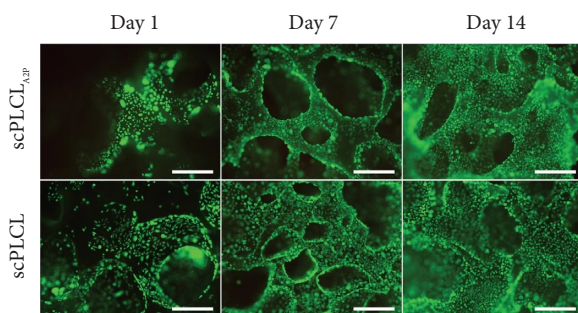

FIGURE 4: Viability of hUCs monoculture on scPLCL$_{A2P}$ and scPLCL at d1, d7, and d14. Viable cells are shown green and dead cells red. Cell growth seems parallel on both scaffolds. Scale bar 500 μm.
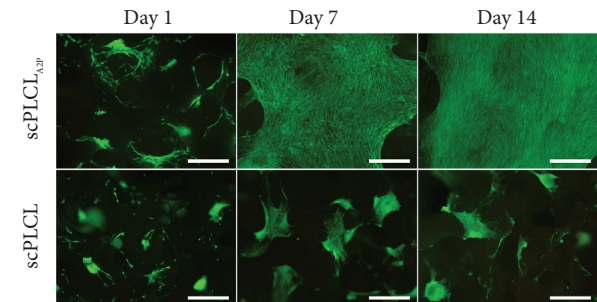

FIGURE 5: Viability of hASCs monoculture on scPLCL$_{A2P}$ and scPLCL at d1, d7, and d14. Viable cells are shown green and dead cells red. The hASCs appear to be spreading more on scPLCL$_{A2P}$ than on scPLCL. Scale bar 500 μm.

on scPLCL, the difference was only two times higher for hASCs.

3.5. scPLCL$_{A2P}$ Supports hUC Phenotype and Enhances hASC αSMA and COL III Expression.

The expression of specific epithelial genes in hUC and stromal genes in hASC monocultures was measured with qRT-PCR on d14 (Figures 11 and 12). The hUC expression of CK7 was significantly increased ($p = 0.004$) on scPLCL$_{A2P}$ compared to

scPLCL. No other statistical significances were detected. However, relative mRNA amounts of urothelial maturation markers UPIa and UPIb both seem slightly higher on scPLCL. The expression of CK8 and CK19 appears similar on both scaffolds.

The expression of stromal markers αSMA, elastin, COL I, COL III, and ratio of expressed COL I/III was determined in hASC monocultures. The amounts of αSMA and COL III mRNA were significantly increased ($p = 0.017$, $p = 0.004$, respectively) in hASCs cultured on scPLCL$_{A2P}$ compared to
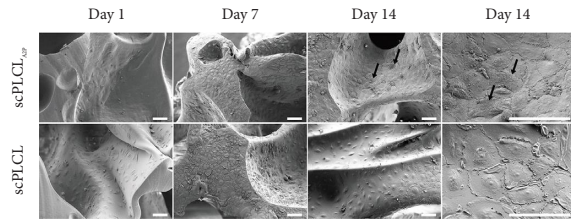
FIGURE 6: Scanning electron microscope (SEM) images showing the morphology of hUCs in monoculture on scPLCL$_{A2P}$ and scPLCL at d1, d7, and d14. Spreading of hUCs seems similar on both scaffolds, yet on d14, the hUCs on scPLCLas seem to have acquired more structural apical surface (arrows). Scale bar 100 μm.

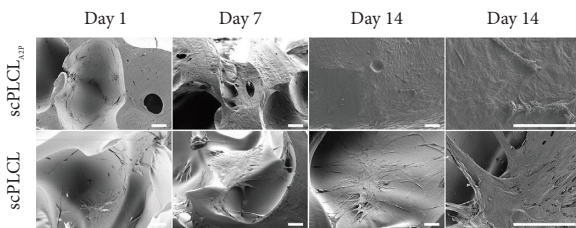FIGURE 7: Scanning electron microscope (SEM) images showing the morphology of hASCs in monoculture on scPLCL$_{A2P}$ and scPLCL at d1, d7, and d14. The hASCs on scPLCL$_{A2P}$ appear to spread more along the scaffold compared to scPLCL. Scale bar 100 μm.
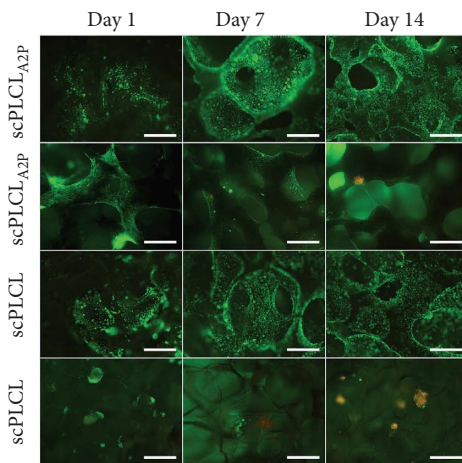

FIGURE 8: Fluorescent images showing the viability of hUCs and hASCs in hUC/hASC coculture on scPLCL$_{A2P}$ and scPLCL at d1, d7, and d14 time points. Viable cells stain green and dead cells red. Cell growth of hUCs remains similar on both scaffolds. Viability of hASCs is supported better on scPLCL$_{A2P}$, whereas hASCs on scPLCL seem to diminish during the coculture. Scale bar 500 μm.

scPLCL. No statistical significances were detected in elastin or COL I expression, and the mRNA amounts appear parallel on both scaffolds. Average ratios of hASC COL I/III mRNA amounts were similar between the scaffolds, 0.6 on scPLCL$_{A2}$ and 0.58 on scPLCL, when examining the Ct-values of the PCR run. No statistical analysis could be done for the COL I/III ratios, as the sample size ($n = 3$) is too small for reliable statistical analysis.

3.6. In Coculture, hUCs Stained for UPIII and hASCs Maintained Myogenic Capabilities on Both Scaffolds. Cell maturation and phenotype maintenance in hUC/hASC coculture on scPLCL$_{A2P}$ and scPLCL were examined with cytochemical and immunofluorescent staining on d14. The costaining of F-actin and pancytokeratin, the acidic and basic cytokeratins detected in epithelial cells, indicates that the hUCs maintained their epithelial phenotype and had similar cortical actin cytoskeleton organization on both scaffolds (Figure 13). Interestingly, the late hUC maturation marker UPIII was stained positive in hUCs on both biomaterials and faintly on PS although the staining was more of a hue than clearly defined area (Figure 14). The actin cytoskeleton of hASCs was organized and aligned on scPLCL$_{A2P}$ and slightly disorganized on scPLCL. Furthermore, αSMA staining in hASCs was superior on scPLCL$_{A2P}$ compared to scPLCL, and very minor staining was detected on control PS.

4. Discussion

The surgical repair of urethral defects currently lacks optimal repair methods as the operations are prone to complications, and suitable autologous donor tissue is scarce [3–5]. To overcome such issues, tissue engineering can be utilized to design biomaterials to mimic the mechanical properties of natural tissues, while also providing optimal niche for tissue regeneration. In this study, we compared two supercritical CO_2-foamed PLCL-based scaffolds, A2P-embedded scPLCL$_{A2P}$, and plain scPLCL, for urethral application. We cultured hUCs and hASCs in mono- and cocultures on porous scPLCL$_{A2P}$ and scPLCL scaffolds to determine the effect of A2P on hUC maturation and on the capability of hASCs to form urethral stromal layer.

Porous scaffolds with interconnected pores allow cell migration into the scaffolds for tissue ingrowth. In this study, we used the process of scCO$_2$-foaming to produce porous scPLCL$_{A2P}$ and scPLCL scaffolds. In scCO$_2$ foaming, the porosity can be adjusted by altering the time, temperature, and pressure during the fabrication process, and no toxic solvents are required [72, 73]. Porous scaffolds produced with scCO$_2$-foaming have previously shown promising results in multiple tissue engineering studies, including in cartilage [22], vaginal [68], and bone [74, 75] applications.

The μCT imaging was performed to show similar scaffold porosity for scPLCL$_{A2P}$ (63%) and scPLCL (69%), with an average pore size of $490 \pm 200 \mu$m and $400 \pm 140 \mu$m, respectively. The measured porosity was in the same range as in previous publications using similar scCO$_2$-foamed PLCL scaffolds [65, 67, 68]. Most importantly, our findings show that the incorporation of A2P did not affect the scaffold porosity, and the pore sizes of both scPLCL$_{A2P}$ and scPLCL are sufficient for cell migration enabling tissue ingrowth. Here, our results indicate that particles up to approximately 400 μm in diameter can enter 50% of the pores in both scPLCL$_{A2P}$ and scPLCL scaffolds, whereas particles up to 200 μm can enter 90% of the pores in both scaffolds. Furthermore, hASCs have been demonstrated to migrate into
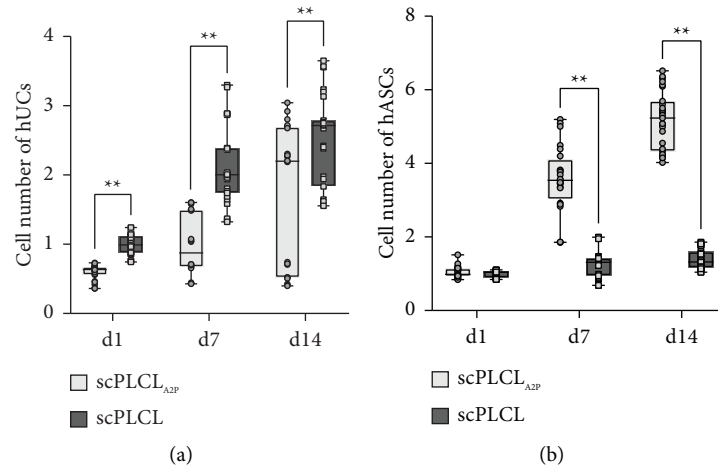
(a)

(b)

FIGURE 9: Cell number of hUC and hASC monocultures relative to d 1 scPLCL CyQUANT mean result ($n = 18$–27). Relative hUC number (a) was significantly higher on scPLCL than on scPLCL$_{A2P}$ at each time point (d1–d 7 $p < 0.001$, d1–d14 $p = 0.009$). On scPLCL$_{A2P}$, the relative hUC number significantly increased between d1–d7 ($p = 0.022$) and d1–d14 ($p = 0.001$). On scPLCL, the hUC number increased d1–d7 and d1–d14 ($p < 0.001$), but no statistical significance was detected between d7–d14 ($p = 0.823$). Relative number of hASCs (b) was similar on both scaffolds on d 1 ($p = 0.27$), but significantly higher on scPLCLas than on scPLCL on d7 and d14 ($p < 0.001$). During the assessment period, relative hASC number on scPLCL$_{A2P}$ increased between each time point (d1–d7 $p < 0.001$, d1–d14 $p < 0.001$, d7–d14 $p < 0.003$). On scPLCL, hASC number increased between d1–d7 ($p = 0.002$) and d1–d14 ($p < 0.001$). ($^{**} = p < 0.01$).
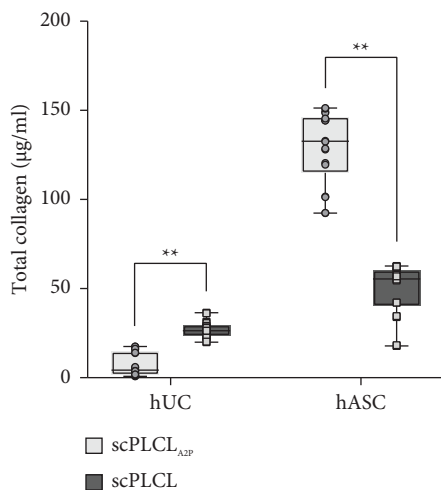

FIGURE 10: Total amount of collagen present in hUC and hASC monocultures on d 14 ($n = 18$). For hUCs, the amount of total collagen was higher on scPLCL compared to scPLCL$_{A2P}$, whereas for hASCs, the total collagen amount was significantly higher on scPLCL$_{A2P}$. ($^{**} = p < 0.01$).

similar scCO$_2$-foamed PLCL scaffolds with a pore size of 350–660 μm [67].

Previously, porous scaffolds embedded with various bioactive components, such as hydroxyapatite and growth factors, have been investigated for tissue engineering applications [75–79]. We wanted to study scPLCL-embedded A2P, as AA has been reported to increase cell proliferation, and it is a critical factor in human collagen synthesis [51, 58]. The scPLCL$_{A2P}$ scaffolds used in this study were incorporated with 8wt-% of A2P. Our previous drug release study using similar porous PLCL scaffolds with 8wt-% A2P revealed that approximately 65% of embedded A2P was

released in 37°C buffer solution during the first week. During the first two weeks, the A2P concentration in solution was 6–85 μg/ml which corresponds to 20–260 μM [65]. Similarly, porous PLGA scaffolds embedded with A2P released 52–66% of A2P during the first 9 days [80]. In addition, electrospun PLA scaffolds were shown to release 50% of the incorporated A2P in distilled water within the first 24 h [60]. Previously, 100 μg/ml AA concentration was reported to be most favourable for hASCs whereas concentrations above 300 μg/ml showed cytotoxic effects [81].

To our knowledge, this is the first study to assess the effect of scaffold embedded A2P on hUC growth and phenotype. The hUCs in monoculture remained viable and proliferated on both scaffolds with no dead cells visible. No apparent difference in hUC viability or spreading could be detected in the Live/Dead assay between scPLCL$_{A2P}$ and scPLCL. Whereas visually the differences in the hUC proliferation on scPLCL$_{A2P}$ and scPLCL scaffolds could not be detected, the quantitative CyQUANT proliferation assay revealed significantly higher hUC amount on scPLCL than on scPLCL$_{A2P}$ at every time point.

We utilized SEM to further study the morphology of hUCs cultured on scaffolds. In SEM images, the hUCs had polygonal cell morphology with well-defined cell borders on both scPLCL$_{A2P}$ and scPLCL. Especially on scPLCL$_{A2P}$, the hUCs had acquired distinctive cell boundaries, possible precursors of tight junction rings. In a natural urothelium, well-defined tight junction rings can be detected around mature umbrella cells, the cells on the mucosal surface of a matured urothelium [82]. In addition, we detected that some hUCs on scPLCL$_{A2P}$ had acquired irregular apical surface which suggests a possible presence of microvilli or urethral plaques, both signs of the UC maturation [82–84]. Formation of tight junctions and presence of microvilli have also been previously reported in tissue engineered
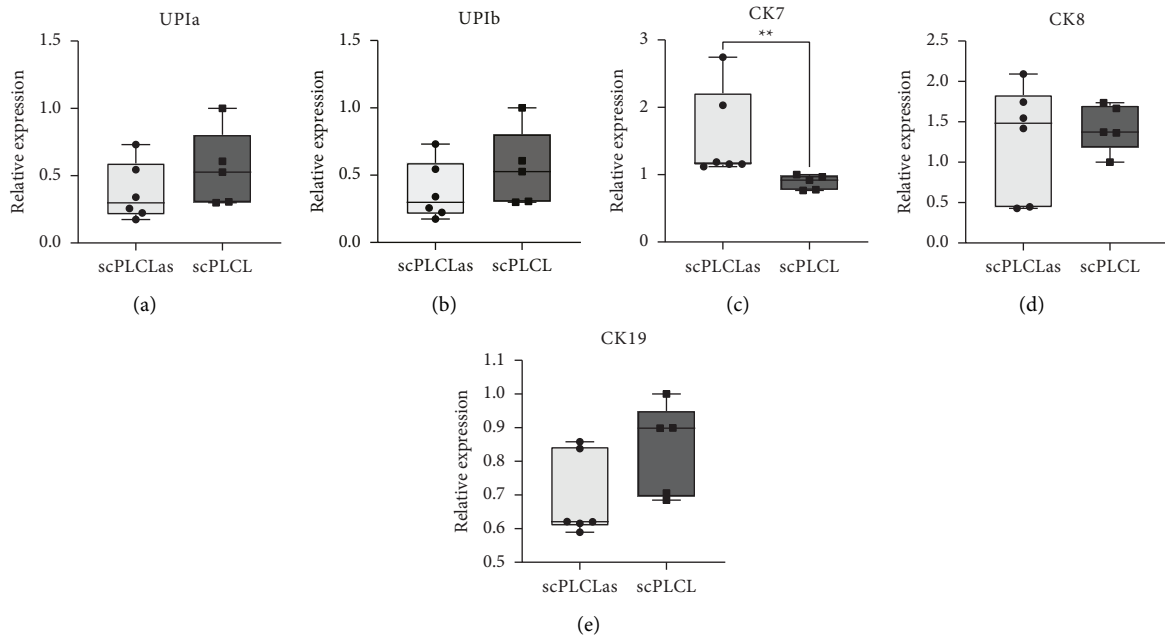
FIGURE 11: The hUC expression of epithelial markers in monoculture on d14 relative to d1 results of a single used donor hUC line. The expression of CK7 mRNA was significantly increased on $scPLCL_{A2P}$ (c). ($p = 0.004$) compared to scPLCL. No significant difference was detected in the expressions of UPIa (a) ($p = 0.329$), UPIb (b) ($p = 0.931$), CK8 (d) ($p = 1.0$), or CK19 (e) ($p = 0.52$) between scaffolds. ($n = 6$, ** $= p < 0.01$).
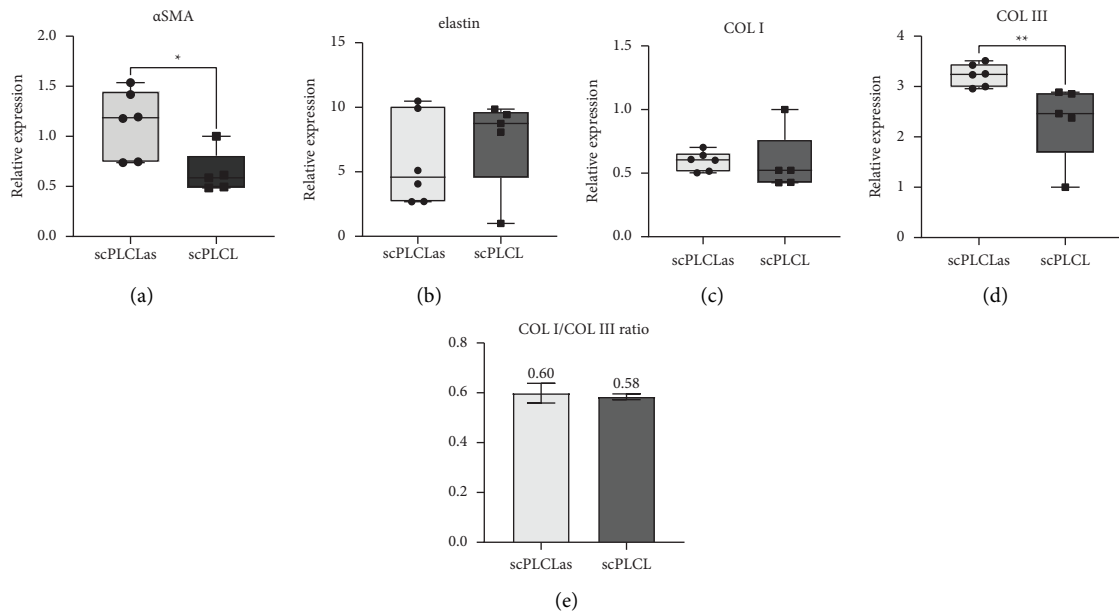

FIGURE 12: The hASC expression of stromal markers in monoculture on d14 relative to d1 results of a single used donor hASC line. The expression of COL III (d) and αSMA (a) mRNA was increased on $scPLCL_{A2P}$ ($p = 0.004$ and 0.017, respectively). No significant difference in COL I (c); ($p = 0.429$) or elastin (b); ($p = 0.931$) mRNA was detected between the scaffolds. Ratio of the expressed COL I/COL III mRNA (e) was similar on both scaffolds. ($n = 6$, * $= p < 0.05$, ** $= p < 0.01$).

urothelium [85, 86]. Therefore, even though the hUC proliferation on $scPLCL_{A2P}$ was significantly lower when compared to scPLCL, the morphology of hUCs on $scPLCL_{A2P}$ could suggest further signs of hUC maturation compared to the hUCs on scPLCL scaffolds.

In addition, our results indicate that the hUCs retained their urothelial phenotype on $scPLCL_{A2P}$ and scPLCL. Importantly, the monocultured hUCs on both scaffolds expressed the UC maturation markers UPIa and UPIb, the major components of the urethral plaques [83, 87].
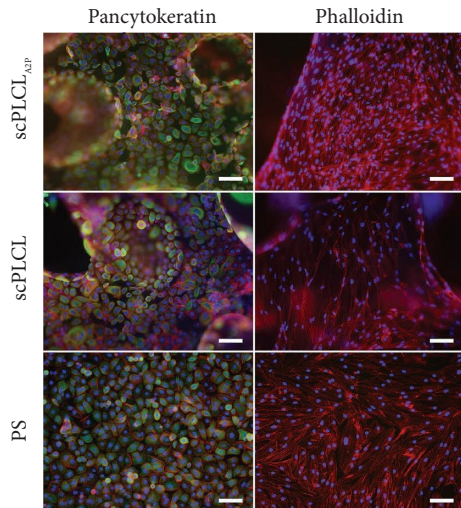
FIGURE 13: Immunofluorescent staining for pancytokeratin (green) and cytochemical staining for F-actin (red) in hUC/hASC coculture on d 14 on scPLCL$_{A2P}$ and scPLCL. The hUCs on the left panel and the hASCs on the right panel. The PS served as a control material. Scale bar 100μm.

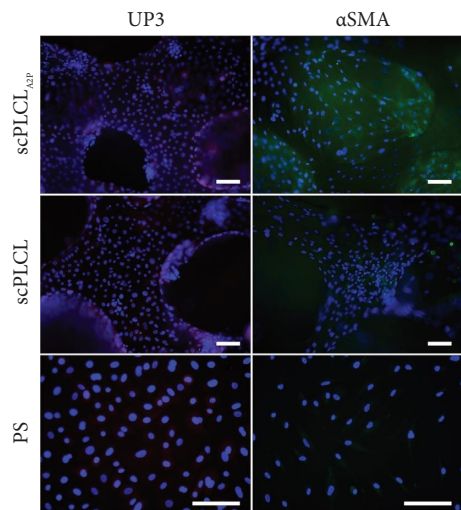
FIGURE 14: Immunofluorescence staining for UPIII (red) in hUCs and for αSMA (green) in hASCs in hUC/hASC coculture on d 14 on scPLCL$_{A2P}$ and scPLCL. hUCs on the left panel and hASCs on the right panel. Control stainings were performed with hUC and hASC monocultures on PS. The hUCs on all materials stain for UPIII. For hASCs, αSMA is present on all materials, yet it seems more abundant on scPLCL$_{A2P}$. Scale bar 100μm.

Particularly, the hUCs on both scPLCL$_{A2P}$ and scPLCL scaffolds expressed the cytokeratins CK7, CK8, and CK19, which are present in the cell layers of a mature urothelium [83, 88]. The amount of expressed CK7 mRNA was significantly higher on scPLCL$_{A2P}$ compared to scPLCL. Even though CK7 is present in all layers of the urethral urothelium, it has been reported to have a critical role in mature umbrella cells and therefore could further indicate the maturation of UCs [88, 89]. We have also previously shown that hUCs cultured on PLCL membranes maintain their

urothelial phenotype and express the cytokeratins CK7, CK8, and CK19 [10] and that vaginal epithelial cells on a scaffold similar to the scPLCL also expressed UPIa, UPIb, and UPIII [68].

Along with the mature urothelium, the regeneration of stromal tissue and smooth muscle layers is critical for functional urethra [26–29], and therefore, we utilized hASC for the stromal compartment in our study. A2P in scPLCL$_{A2P}$ had a noticeable effect on hASC viability and proliferation. Our results show how cells in the hASC monoculture proliferated and spread densely over the scPLCL$_{A2P}$ scaffold, whereas on scPLCL, the hASCs formed clusters. The dense spreading of hASCs on scPLCL$_{A2P}$ and clustering on scPLCL was also visible in SEM imaging. Such clustering on scPLCL scaffolds was also seen in our previous study using human vaginal stromal cells [68]. One possible explanation for cell clustering could be the hydrophobicity of the PLCL [90] hindering the hASC attachment and forcing them to form clusters with each other. The incorporation of A2P could decrease the hydrophobicity of PLCL and therefore allow better cell attachment, as also demonstrated for PLA scaffolds [60]. The striking effect on hASC proliferation was also observed in CyQUANT proliferation assay, where the hASCs on scPLCL$_{A2P}$ kept proliferating the entire 14-d assessing period, and the number of hASCs remained superior when compared to scPLCL at each time point. Therefore, in contrast to hUCs, the A2P in scPLCL$_{A2P}$ strongly enhances the hASC proliferation.

Even though A2P enhanced the hASC proliferation in our study, too high concentrations of AA or A2P in cell culture have been suggested to lead to cytotoxicity and reduced viability [58, 81, 91], although contradictory reports have been published. For hASCs, cytotoxicity of supplemented A2P appears to be dose-dependent and could be prevented by increasing the cell density. Moreover, AA was more cytotoxic than A2P. Concentration of 250μM A2P supplemented in the cell culture medium has been reported to be beneficial for hASC proliferation, stemness, and collagen synthesis [53], but cytotoxicity has also been detected with the same 250μM concentration [91]. The 250μM concentration has also shown to increase proliferation of bone marrow-derived mesenchymal stem cells [58].

Collagen is the major component of stromal ECM, and both AA and A2P can stimulate its production and enhance the collagen mRNA expression and stability [50, 92–94]. Therefore, we assessed the effect of scPLCL$_{A2P}$ on the total amount of collagen in hUC and hASC monocultures. The amount of collagen in hUC monoculture was lower on scPLCL$_{A2P}$ compared to scPLCL; however, epithelial cells are not expected to produce high quantities of collagen [95, 96]. Instead, the A2P significantly increased the total amount of collagen in hASC monocultures. However, the increase could not be detected in the COL I mRNA levels, yet the amount of hASC COL III mRNA was increased on scPLCL$_{A2P}$. Therefore, as 90% of produced collagen is COL I [50], the effect of A2P in scPLCL$_{A2P}$ seems to be associated with the COL I maturation rather than in the mRNA expression. Previously, supplemented AA or its derivatives have been shown to increase the collagen production in

hASCs and bone marrow-derived stem cells [53, 55, 58, 81], and similarly to our findings, COL III mRNA but not COL I mRNA expression was increased in A2P-supplemented osteoblasts [97]. However, Yu et al. reported an increase in both total collagen and COL I mRNA amounts in hASCs cultured with supplemented A2P [53].

Increased amount of COL III may provide more elasticity for the forming tissue [98, 99], but overproduction of COL III may contribute to the formation of fibrosis [99, 100]. Decreased ratio of COL I/III in tissue has been identified in fibrotic growth [101, 102]. Therefore, the amount of COL III formed and the ratio of COL I and COL III in situ are important as abnormal ratio may lead to stiffness or fibrosis in the forming tissue. In our current study, the hASCs COL I/III mRNA ratio was very similar in hASC cultured on scPLCL$_{A2P}$ (0.60) and on scPLCL (0.58). For both, the ratio was less than one, meaning more COL III to COL I mRNA was detected on both scaffolds. The significance of the increased COL III mRNA should be investigated in more detail in future research.

In this study, we established hUC and hASC cocultures to represent the layers of a natural urethra by seeding the cell types on the opposite sides of the scaffold. The hUCs cultured on top of the scaffold represent the urothelium. The scaffold functions as a temporary lamina propria for the hUCs to attach to and the hASCs seeded on the opposite side represent the stromal layer underlying the lamina propria. Previously, hUCs have been cocultured with various cell types, including fibroblasts and smooth muscle cells [103], and hASCs [81, 104]. In our study, we utilized pediatric primary hUCs, whereas in many previously published studies, adult or age unspecified hUCs have been used [85, 86, 104, 105]. However, also the adult-derived hUCs have been demonstrated to retain their capacity to form functional urothelium [86, 105]. Our results show that the hUCs remained viable in the coculture with hASCs on both scPLCL$_{A2P}$ and scPLCL scaffolds. The hUC viability in coculture with hASCs was similar on both scaffolds and appeared alike to the hUCs in monoculture.

Most importantly, our results revealed that the hUCs maintained their phenotype also in the coculture with hASCs. The hUCs on both scaffolds stained positive for pancytokeratin, the cytokeratins presented by epithelial cells. Notably, staining of the late hUC maturation marker UPIII appeared to be higher in the hUCs on the scPLCL$_{A2P}$ and scPLCL scaffolds, whereas only a dim staining was detected on control PS. In a previous study, the expression of UPIII, UPIa, or UPIb was not detected in hUCs under static culture conditions [85] or when cocultured on an ASC-basedself-assembled scaffold [86]. However, when cultured on a combination of fibroblast and ASC-basedself-assembled scaffold, UPIa-, UPIb-, and UPIII-positive hUCs were detected [86]. In contrast, a more recent study reported that hUCs cultured on self-assembled hASC scaffold did maintain their phenotype and expressed the specific markers UPIa, UPIb, CK7, and CK20 [81]. Previously, hUCs have also been cocultured with hASCs to induce hASC urothelial differentiation [104]. The hASCs expressed UPIb and UPII in a direct hUC coculture, whereas they were not detected in an in-direct coculture [104].

We observed that the A2P in scPLCL$_{A2P}$ supported the hASC growth also in coculture despite the used suboptimal coculture medium, whereas on scPLCL, the viable hASCs seem to gradually diminish. Viable hASC sheet is visible on scPLCL$_{A2P}$ also at d14, although the strong hue of hUC staining through the scaffold partly conceals the signal of hASCs. These findings verify the results of the hASC monocultures and are also supported by previous research, where AA and its derivatives have been shown to significantly increase the proliferation rate of human mesenchymal stem cells, including hASCs [53, 58, 106–108]. Additionally, we studied the presence of hASCs in hUC/hASC cocultures with F-actin cytoskeleton staining. This staining also illustrated enhanced hASC growth and spreading on the scPLCL$_{A2P}$ scaffold compared to scPLCL. For the hUCs, actin staining showed similar cortical organization on both scaffolds.

In the current study, more αSMA mRNA was measured in hASC monocultures on scPLCL$_{A2P}$, and more αSMA-positive hASCs were detected in coculture on scPLCL$_{A2P}$ when compared to scPLCL. Increased αSMA expression in ASCs has been linked to enhanced myogenic differentiation [47]. Furthermore, increased hASC and fibroblast αSMA expression has been reported when cultured with AA [109, 110]. Therefore, in our study, the A2P in scPLCL$_{A2P}$ may have enhanced the myogenic capacity of hASCs. However, in addition to indicating smooth muscle cell differentiation and presence of smooth muscle cells, αSMA is expressed by myofibroblasts [111]. It may also indicate pericytic and proangiogenic functions of hASC [112].

5. Conclusions

We demonstrated the potential of scPLCL$_{A2P}$ scaffolds for urethral tissue engineering applications. The novel scPLCL$_{A2P}$ scaffold supported the viability of both hUCs and hASCs in mono- and coculture, even despite the suboptimal coculturing conditions for hASCs. All our results support the cytocompatibility and bio-compatibility of the scPLCL$_{A2P}$ scaffolds, yet future in vivo experiments are still required to further ensure their safety. The effect of A2P on hUCs was modest, yet most importantly, the hUCs maintained their phenotype and expressed urothelial maturation markers both in mono- and coculture. We were able to show UPIa, UPIb, and UPIII expression in hUCs; however, further research is needed to explore the hUC maturation in more detail. The proliferation and collagen production of hASCs were significantly increased on scPLCL$_{A2P}$ when compared to scPLCL. However, more research on the effect of A2P on COL I and COL III production is needed to detect and avoid the formation of fibrosis. Moreover, αSMA expression in hASC was increased on scPLCL$_{A2P}$, possibly suggesting an increased myogenic or proangiogenic potential. For future research, the coculture conditions need to be optimized to better support both hUCs and hASCs to allow further assessment of hUC maturation and hASC stromal production on the scPLCL$_{A2P}$ scaffolds.

Data Availability

The data that support the findings of this study are available from the corresponding author upon reasonable request.

Conflicts of Interest

The authors declare that there are no conflicts of interest.

Authors' Contributions

A. K carried out all in vitro cell work, analysis of data and writing of the original draft, manuscript review, and editing; K. P developed scaffold design and fabrication, and manuscript review; M. H carried out μCT imaging and data processing, and manuscript review; J. H carried out μCT imaging review and manuscript review; S. M developed conceptualization, supervision, funding acquisition, manuscript review, and editing; R. S developed conceptualization, study design, supervision, funding acquisition, manuscript review, and editing.

References

[1] R. A. Santucci, G. F. Joyce, and M. Wise, "Male urethral stricture disease," *The Journal of Urology*, vol. 177, no. 5, pp. 1667–1674, 2007.

[2] M. Lazzeri, S. Sansalone, G. Guazzoni, and G. Barbagli, "Incidence, causes, and complications of urethral stricture disease," *European Urology Supplements*, vol. 15, no. 1, pp. 2–6, 2016.

[3] H. J. R. van der Horst and L. L. de Wall, "Hypospadias, all there is to know," *European Journal of Pediatrics*, vol. 176, no. 4, pp. 435–441, 2017.

[4] D. D. Dugi, J. Simhan, and A. F. Morey, "Urethroplasty for stricture disease: contemporary techniques and outcomes," *Urology*, vol. 89, pp. 12–18, 2016.

[5] L. R. M. Versteegden, P. K. J. D. de Jonge, J. IntHout et al., "Tissue engineering of the urethra: a systematic review and meta-analysis of preclinical and clinical studies," *European Urology*, vol. 72, no. 4, pp. 594–606, 2017.

[6] N. Mangir, K. J. Wilson, N. I. Osman, and C. R. Chapple, "Current state of urethral tissue engineering," *Current Opinion in Urology*, vol. 29, no. 4, pp. 385–393, 2019.

[7] T. O. Abbas, H. C. Yalcin, and C. P. Pennisi, "From acellular matrices to smart polymers: degradable scaffolds that are transforming the shape of urethral tissue engineering," *International Journal of Molecular Sciences*, vol. 20, no. 7, 2019.

[8] V. De Kemp, P. De Graaf, J. O. Fledderus, J. L. H. Ruud Bosch, and L. M. O. De Kort, "Tissue engineering for human urethral reconstruction: systematic review of recent literature," *PLoS One*, vol. 10, no. 2, Article ID e0118653, 2015.

[9] N. F. Davis, E. M. Cunnane, F. J. O'Brien, J. J. Mulvihill, and M. T. Walsh, "Tissue engineered extracellular matrices (ECMs) in urology: evolution and future directions," *The Surgeon*, vol. 16, no. 1, pp. 55–65, 2018.

[10] R. Sartoneva, S. Haimi, S. Miettinen et al., "Comparison of a poly-L-lactide-co-ε-caprolactone and human amniotic membrane for urothelium tissue engineering applications," *Journal of The Royal Society Interface*, vol. 8, no. 58, pp. 671–677, 2011.

[11] Q. Yao, W. Zhang, Y. Hu et al., "Electrospun collagen/poly(L-lactic acid-co-ε-caprolactone) scaffolds for conjunctival tissue engineering," *Experimental and Therapeutic Medicine*, vol. 14, no. 5, pp. 4141–4147, 2017.

[12] C. P. Laurent, C. Vaquette, X. Liu, J. F. Schmitt, and R. Rahouadj, "Suitability of a PLCL fibrous scaffold for soft tissue engineering applications: a combined biological and mechanical characterisation," *Journal of Biomaterials Applications*, vol. 32, no. 9, pp. 1276–1288, 2018.

[13] A. I. Pangesty, T. Arahira, and M. Todo, "Development and characterization of hybrid tubular structure of PLCL porous scaffold with hMSCs/ECs cell sheet," *Journal of Materials Science: Materials in Medicine*, vol. 28, no. 10, 2017.

[14] C. Zhu, X. Wu, Y. Wang et al., "Preclinical animal study and human clinical trial data of co-electrospun poly(L-lactide-co-caprolactone) and fibrinogen mesh for anterior pelvic floor reconstruction," *International Journal of Nanomedicine*, vol. 11, pp. 389–397, 2016.

[15] R. Sartoneva, P. H. Nordback, S. Haimi et al., "Comparison of poly(l-lactide-co-ϵ-caprolactone) and poly(trimethylene carbonate) membranes for urethral regeneration: an in vitro and in vivo study," *Tissue Engineering Part A*, vol. 24, no. 1-2, pp. 117–127, 2018.

[16] A. Kurki, "Use of poly(L-lactide-co-ε-caprolactone) based biomaterials in urological and gynaecological tissue engineering applications," M.Sc. thesis, Tampere University, Tampere, Finland, 2019.

[17] J. Fernández, A. Etxeberria, and J. R. Sarasua, "Synthesis, structure and properties of poly(L-lactide-co-ε-caprolactone) statistical copolymers," *Journal of the Mechanical Behavior of Biomedical Materials*, vol. 9, pp. 100–112, 2012.

[18] L. S. Nair and C. T. Laurencin, "Biodegradable polymers as biomaterials," *Progress in Polymer Science*, vol. 32, no. 8-9, pp. 762–798, 2007.

[19] S. Saad, N. I. Osman, and C. R. Chapple, "Tissue engineering: recent advances and review of clinical outcome for urethral strictures," *Current Opinion in Urology*, vol. 31, no. 5, pp. 498–503, 2021.

[20] Y. Y. Chan, M. I. Bury, E. M. Yura, M. D. Hofer, E. Y. Cheng, and A. K. Sharma, "The current state of tissue engineering in the management of hypospadias," *Nature Reviews Urology*, vol. 17, no. 3, pp. 162–175, 2020.

[21] S. I. Jeong, S. H. Kim, Y. H. Kim et al., "Manufacture of elastic biodegradable PLCL scaffolds for mechano-active vascular tissue engineering," *Journal of Biomaterials Science, Polymer Edition*, vol. 15, no. 5, pp. 645–660, 2004.

[22] S. H. Kim, Y. Jung, and S. H. Kim, "A biocompatible tissue scaffold produced by supercritical fluid processing for

cartilage tissue engineering," *Tissue Engineering Part C Methods*, vol. 19, no. 3, pp. 181–188, 2013.

[23] Z. Lv, N. Zhao, Z. Wu, C. Zhu, and Q. Li, "Fabrication of novel open-cell foams of poly(ε-caprolactone)/poly(lactic acid) blends for tissue-engineering scaffolds," *Industrial and Engineering Chemistry Research*, vol. 57, no. 39, pp. 12951–12958, 2018.

[24] C. Song, Y. Luo, Y. Liu et al., "Fabrication of PCL scaffolds by supercritical CO2 foaming based on the combined effects of rheological and crystallization properties," *Polymers*, vol. 12, no. 4, 2020.

[25] K. Kosowska, J. Krzysztoforski, and M. Henczka, "Foaming of PCL-based composites using scCO2: structure and physical properties," *Materials*, vol. 15, no. 3, 2022.

[26] H. Orabi, T. Aboushwareb, Y. Zhang, J. J. Yoo, and A. Atala, "Cell-seeded tubularized scaffolds for reconstruction of long urethral defects: a preclinical study," *European Urology*, vol. 63, no. 3, pp. 531–538, 2013.

[27] R. E. De Filippo, B. S. Kornitzer, J. J. Yoo, and A. Atala, "Penile urethra replacement with autologous cell-seeded tubularized collagen matrices," *Journal of Tissue Engineering and Regenerative Medicine*, vol. 9, no. 3, pp. 257–264, 2015.

[28] M. V. Amesty, C. I. Chamorro, P. López-Pereira et al., "Creation of tissue-engineered urethras for large urethral defect repair in a rabbit experimental model," *Frontiers in Pediatrics*, vol. 9, Article ID 691131, 2021.

[29] H. Zhong, Y. Shen, D. Zhao et al., "Cell-seeded acellular artery for reconstruction of long urethral defects in a canine model," *Stem Cells International*, vol. 2021, Article ID 8854479, 9 pages, 2021.

[30] L. F. Arenas Da Silva, L. Micol, D. Tiemessen et al., "Is there a need for smooth muscle cell transplantation in urethral reconstruction?" *Tissue Engineering Part A*, vol. 20, no. 9-10, pp. 1542–1549, 2014.

[31] S. Bhargava, C. R. Chapple, A. J. Bullock, C. Layton, and S. Macneil, "Tissue-engineered buccal mucosa for substitution urethroplasty," *BJU International*, vol. 93, no. 6, pp. 807–811, 2004.

[32] S. Zhou, R. Yang, Q. Zou et al., "Fabrication of tissue-engineered bionic urethra using cell sheet technology and labeling by ultrasmall superparamagnetic iron oxide for full-thickness urethral reconstruction," *Theranostics*, vol. 7, no. 9, pp. 2509–2523, 2017.

[33] C. Wang, C. Chen, M. Guo, B. Li, F. Han, and W. Chen, "Stretchable collagen-coatedpolyurethane-urea hydrogel seeded with bladder smooth muscle cells for urethral defect repair in a rabbit model," *Journal of Materials Science: Materials in Medicine*, vol. 30, no. 12, 2019.

[34] Y. Niu, G. Liu, C. Chen et al., "Urethral reconstruction using an amphiphilic tissue-engineered autologous polyurethane nanofiber scaffold with rapid vascularization function," *Biomaterials Science*, vol. 8, no. 8, pp. 2164–2174, 2020.

[35] S. Wu, Y. Liu, S. Bharadwaj, A. Atala, and Y. Zhang, "Human urine-derived stem cells seeded in a modified 3D porous small intestinal submucosa scaffold for urethral tissue engineering," *Biomaterials*, vol. 32, no. 5, pp. 1317–1326, 2011.

[36] B. Tian, L. Song, T. Liang et al., "Repair of urethral defects by an adipose mesenchymal stem cell-porous silk fibroin

material," *Molecular Medicine Reports*, vol. 18, no. 1, pp. 209–215, 2018.

[37] H. Li, Y. Xu, H. Xie et al., "Epithelial-differentiatedadipose-derived stem cells seeded bladder acellular matrix grafts for urethral reconstruction: an animal model," *Tissue Engineering Part A*, vol. 20, no. 3-4, pp. 774–784, 2014.

[38] C. L. Li, W. B. Liao, S. X. Yang et al., "Urethral reconstruction using bone marrow mesenchymal stem cell- and smooth muscle cell-seeded bladder acellular matrix," *Transplantation Proceedings*, vol. 45, no. 9, pp. 3402–3407, 2013.

[39] A. Raya-Rivera, D. R. Esquiliano, J. J. Yoo, E. Lopez-Bayghen, S. Soker, and A. Atala, "Tissue-engineered autologous urethras for patients who need reconstruction: an observational study," *The Lancet*, vol. 377, no. 9772, pp. 1175–1182, 2011.

[40] M. Fossum, J. Svensson, G. Kratz, and A. Nordenskjöld, "Autologous in vitro cultured urothelium in hypospadias repair," *Journal of Pediatric Urology*, vol. 3, no. 1, pp. 10–18, 2007.

[41] J. Southgate, J. R. W. Masters, and L. K. Trejdosiewicz, "Culture of human urothelium," in *Culture of Epithelial Cells*, R. I. Freshney and M. G. Freshney, Eds., Wiley-Liss, Inc, New York, NY, USA, 2003.

[42] R. Sartoneva, A. M. Haaparanta, T. Lahdes-Vasama et al., "Characterizing and optimizing poly- l -lactide-co-ε-caprolactone membranes for urothelial tissue engineering," *Journal of The Royal Society Interface*, vol. 9, no. 77, pp. 3444–3454, 2012.

[43] U. Nagele, S. Maurer, G. Feil et al., "In vitro investigations of tissue-engineered multilayered urothelium established from bladder washings," *European Urology*, vol. 54, no. 6, pp. 1414–1422, 2008.

[44] M. Fossum, C. J. Gustafson, A. Nordenskjöld, and G. Kratz, "Isolation and in vitro cultivation of human urothelial cells from bladder washings of adult patients and children," *Scandinavian Journal of Plastic and Reconstructive Surgery and Hand Surgery*, vol. 37, no. 1, pp. 41–45, 2003.

[45] B. Walters, P. A. Turner, B. Rolauffs, M. L. Hart, and J. P. Stegemann, "Controlled growth factor delivery and cyclic stretch induces a smooth muscle cell-like phenotype in adipose-derived stem cells," *Cells*, vol. 10, no. 11, 2021.

[46] L. V. Rodríguez, Z. Alfonso, R. Zhang, J. Leung, B. Wu, and L. J. Ignarro, "Clonogenic multipotent stem cells in human adipose tissue differentiate into functional smooth muscle cells," *Proceedings of the National Academy of Sciences of the United States of America*, vol. 103, no. 32, Article ID 12167, 2006.

[47] C. Wang, S. Yin, L. Cen et al., "Differentiation of adipose-derived stem cells into contractile smooth muscle cells induced by transforming growth factor-β1 and bone morphogenetic protein-4," *Tissue Engineering Part A*, vol. 16, no. 4, pp. 1201–1213, 2010.

[48] J. Zhang, Y. Liu, Y. Chen et al., "Adipose-derived stem cells: current applications and future directions in the regeneration of multiple tissues," *Stem Cells International*, vol. 2020, Article ID 8810813, 26 pages, 2020.

[49] Y. Wang, X. Chen, W. Cao, and Y. Shi, "Plasticity of mesenchymal stem cells in immunomodulation: pathological and therapeutic implications," *Nature Immunology*, vol. 15, no. 11, pp. 1009–1016, 2014.

[50] O. Arrigoni and M. C. De Tullio, "Ascorbic acid: much more than just an antioxidant," *Biochimica et Biophysica Acta (BBA) - General Subjects*, vol. 1569, no. 1-3, pp. 1–9, 2002.

[51] C. D'Aniello, F. Cermola, E. J. Patriarca, and G. Minchiotti, "Vitamin C in stem cell biology: impact on extracellular matrix homeostasis and epigenetics," *Stem Cells International*, vol. 2017, Article ID 8936156, 16 pages, 2017.

[52] Y. Kishimoto, N. Saito, K. Kurita, K. Shimokado, N. Maruyama, and A. Ishigami, "Ascorbic acid enhances the expression of type 1 and type 4 collagen and SVCT2 in cultured human skin fibroblasts," *Biochemical and Biophysical Research Communications*, vol. 430, no. 2, pp. 579–584, 2013.

[53] J. Yu, Y. K. Tu, Y. B. Tang, and N. C. Cheng, "Stemness and transdifferentiation of adipose-derived stem cells using L-ascorbic acid 2-phosphate-induced cell sheet formation," *Biomaterials*, vol. 35, no. 11, pp. 3516–3526, 2014.

[54] A. Tanaka, T. Hasegawa, K. Morimoto et al., "Controlled release of ascorbic acid from gelatin hydrogel attenuates abdominal aortic aneurysm formation in rat experimental abdominal aortic aneurysm model," *Journal of Vascular Surgery*, vol. 60, no. 3, pp. 749–758, 2014.

[55] J. Y. Zhang, B. A. Doll, E. J. Beckman, and J. O. Hollinger, "Three-Dimensional biocompatible ascorbic acid-containing scaffold for bone tissue engineering," *Tissue Engineering*, vol. 9, no. 6, pp. 1143–1157, 2003.

[56] S. Takamizawa, Y. Maehata, K. Imai, H. Senoo, S. Sato, and R. I. Hata, "Effects of ascorbic acid and ascorbic acid 2-phosphate, a long-acting vitamin C derivative, on the proliferation and differentiation of human osteoblast-like cells," *Cell Biology International*, vol. 28, no. 4, pp. 255–265, 2004.

[57] T. Takahashi, B. Lord, P. C. Schulze et al., "Ascorbic acid enhances differentiation of embryonic stem cells into cardiac myocytes," *Circulation*, vol. 107, no. 14, pp. 1912–1916, 2003.

[58] K. M. Choi, Y. K. Seo, H. H. Yoon et al., "Effect of ascorbic acid on bone marrow-derived mesenchymal stem cell proliferation and differentiation," *Journal of Bioscience and Bioengineering*, vol. 105, no. 6, pp. 586–594, 2008.

[59] M. G. Perino, S. Yamanaka, D. R. Riordon, Y. Tarasova, and K. R. Boheler, "Ascorbic acid promotes cardiomyogenesis through SMAD1 signaling in differentiating mouse embryonic stem cells," *PLoS One*, vol. 12, no. 12, Article ID e0188569, 2017.

[60] N. Mangir, A. J. Bullock, S. Roman, N. Osman, C. Chapple, and S. MacNeil, "Production of ascorbic acid releasing biomaterials for pelvic floor repair," *Acta Biomaterialia*, vol. 29, pp. 188–197, 2016.

[61] S. Haimi, N. Suuriniemi, A. M. Haaparanta et al., "Growth and osteogenic differentiation of adipose stem cells on PLA/bioactive glass and PLA/β-TCP scaffolds," *Tissue Engineering Part A*, vol. 15, no. 7, pp. 1473–1480, 2009.

[62] L. Kyllönen, S. Haimi, B. Mannerström et al., "Effects of different serum conditions on osteogenic differentiation of human adipose stem cells in vitro," *Stem Cell Research and Therapy*, vol. 4, no. 1, 2013.

[63] M. Dominici, K. Le Blanc, I. Mueller et al., "Minimal criteria for defining multipotent mesenchymal stromal cells. The International Society for Cellular Therapy position statement," *Cytotherapy*, vol. 8, no. 4, pp. 315–317, 2006.

[64] M. Patrikoski, B. Mannerström, and S. Miettinen, "Perspectives for clinical translation of adipose stromal/stem cells," *Stem Cells International*, vol. 2019, Article ID 5858247, 21 pages, 2019.

[65] S. Asikainen, K. Paakinaho, A. K. Kyhkynen et al., "Hydrolysis and drug release from poly(ethylene glycol)-modified lactone polymers with open porosity," *European Polymer Journal*, vol. 113, pp. 165–175, 2019.

[66] M. Doube, M. M. Klosowski, I. Arganda-Carreras et al., "BoneJ: free and extensible bone image analysis in ImageJ," *Bone*, vol. 47, no. 6, pp. 1076–1079, 2010.

[67] A. Palmroth, S. Pitkänen, M. Hannula et al., "Evaluation of scaffold microstructure and comparison of cell seeding methods using micro-computedtomography-based tools," *Journal of The Royal Society Interface*, vol. 17, no. 165, Article ID 20200102, 2020.

[68] R. Sartoneva, K. Kuismanen, M. Juntunen et al., "Porous (poly-L-lactide-co-epsilon-caprolactone) scaffold: a novel biomaterial for vaginal tissue engineering," *Royal Society Open Science*, vol. 5, no. 8, Article ID 180811, 2018.

[69] K. Vuornos, M. Björninen, E. Talvitie et al., "Human adipose stem cells differentiated on braided polylactide scaffolds is a potential approach for tendon tissue engineering," *Tissue Engineering Part A*, vol. 22, no. 5-6, pp. 513–523, 2016.

[70] K. Vuornos, H. Huhtala, M. Kääriäinen et al., "Bioactive glass ions for in vitro osteogenesis and microvascularization in gellan gum-collagen hydrogels," *Journal of Biomedical Materials Research Part B: Applied Biomaterials*, vol. 108, no. 4, pp. 1332–1342, 2020.

[71] C. Becker, A. Hammerle-Fickinger, I. Riedmaier, and M. W. Pfaffl, "mRNA and microRNA quality control for RT-qPCR analysis," *Methods*, vol. 50, no. 4, pp. 237–243, 2010.

[72] M. Castano, E. Martinez-Campos, M. Pintado-Sierra et al., "Combining breath figures and supercritical fluids to obtain porous polymer scaffolds," *ACS Omega*, vol. 3, no. 10, Article ID 12593, 2018.

[73] H. Tai, M. L. Mather, D. Howard et al., "Control of pore size and structure of tissue engineering scaffolds produced by supercritical fluid processing," *European Cells and Materials*, vol. 14, pp. 64–77, 2007.

[74] S. Pitkänen, K. Paakinaho, H. Pihlman et al., "Characterisation and in vitro and in vivo evaluation of supercritical-CO2-foamed β-TCP/PLCL composites for bone applications," *European Cells and Materials*, vol. 38, pp. 35–50, 2019.

[75] V. E. Santo, A. R. C. Duarte, E. G. Popa, M. E. Gomes, J. F. Mano, and R. L. Reis, "Enhancement of osteogenic differentiation of human adipose derived stem cells by the controlled release of platelet lysates from hybrid scaffolds produced by supercritical fluid foaming," *Journal of Controlled Release*, vol. 162, no. 1, pp. 19–27, 2012.

[76] T. Zhu, M. Jiang, M. Zhang et al., "Biofunctionalized composite scaffold to potentiate osteoconduction, angiogenesis, and favorable metabolic microenvironment for osteonecrosis therapy," *Bioactive Materials*, vol. 9, pp. 446–460, 2022.

[77] Z. Liu, J. Zhang, C. Fu, and J. Ding, "Osteoimmunity-regulating biomaterials promote bone regeneration," *Asian Journal of Pharmaceutical Sciences*, vol. 18, no. 1, Article ID 100774, 2023.

[78] T. Zhu, M. Jiang, M. Zhang et al., "Construction and validation of steroid-induced rabbit osteonecrosis model," *MethodsX*, vol. 9, Article ID 101713, 2022.

[79] D. Zhao, T. Zhu, J. Li et al., "Poly(lactic-co-glycolic acid)-based composite bone-substitute materials," *Bioactive Materials*, vol. 6, no. 2, pp. 346–360, 2021.

[80] H. Kim, H. W. Kim, and H. Suh, "Sustained release of ascorbate-2-phosphate and dexamethasone from porous PLGA scaffolds for bone tissue engineering using mesenchymal stem cells," *Biomaterials*, vol. 24, no. 25, pp. 4671–4679, 2003.

[81] Z. Rashidbenam, M. H. Jasman, G. H. Tan et al., "Fabrication of adipose-derived stem cell-basedself-assembled scaffold under hypoxia and mechanical stimulation for urethral tissue engineering," *International Journal of Molecular Sciences*, vol. 22, no. 7, 2021.

[82] G. Apodaca, "The uroepithelium: not just a passive barrier," *Traffic*, vol. 5, no. 3, pp. 117–128, 2004.

[83] P. Khandelwal, S. N. Abraham, and G. Apodaca, "Cell biology and physiology of the uroepithelium," *American Journal of Physiology - Renal Physiology*, vol. 297, no. 6, Article ID F1477, 2009.

[84] M. G. Dalghi, N. Montalbetti, M. D. Carattino, and G. Apodaca, "The urothelium: Life in a liquid environment," *Physiological Reviews*, vol. 100, no. 4, pp. 1621–1705, 2020.

[85] V. Cattan, G. Bernard, A. Rousseau et al., "Mechanical stimuli-induced urothelial differentiation in a human tissue-engineered tubular genitourinary graft," *European Urology*, vol. 60, no. 6, pp. 1291–1298, 2011.

[86] A. Rousseau, J. Fradette, G. Bernard, R. Gauvin, V. Laterreur, and S. Bolduc, "Adipose-derived stromal cells for the reconstruction of a human vesical equivalent," *Journal of Tissue Engineering and Regenerative Medicine*, vol. 9, no. 11, pp. E135–E143, 2015.

[87] A. R. Carpenter, M. B. Becknell, C. B. Ching et al., "Uroplakin 1b is critical in urinary tract development and urothelial differentiation and homeostasis," *Kidney International*, vol. 89, no. 3, pp. 612–624, 2016.

[88] J. Southgate, P. Harnden, and L. K. Trejdosiewicz, "Cytokeratin expression patterns in normal and malignant urothelium: a review of the biological and diagnostic implications," *Histology and Histopathology*, vol. 14, no. 2, pp. 657–664, 1999.

[89] P. Veranič and K. Jezernik, "Trajectorial organisation of cytokeratins within the subapical region of umbrella cells," *Cell Motility and the Cytoskeleton*, vol. 53, no. 4, pp. 317–325, 2002.

[90] K. Webb, V. Hlady, and P. A. Tresco, "Relative importance of surface wettability and charged functional groups on NIH 3T3 fibroblast attachment, spreading, and cytoskeletal organization," *Journal of Biomedical Materials Research*, vol. 41, no. 3, pp. 422–430, 1998.

[91] Y. K. Wu, Y. K. Tu, J. Yu, and N. C. Cheng, "The influence of cell culture density on the cytotoxicity of adipose-derived stem cells induced by L-ascorbic acid-2-phosphate," *Scientific Reports*, vol. 10, no. 1, 2020.

[92] R.-I. Hata and H. Senoo, "L-ascorbic acid 2-phosphate stimulates collagen accumulation, cell proliferation, and formation of a three-dimensional tissuelike substance by skin fibroblasts," *Journal of Cellular Physiology*, vol. 138, no. 1, pp. 8–16, 1989.

[93] J. M. Davidson, P. A. LuValle, O. Zoia, D. Quaglino, and M. Giro, "Ascorbate differentially regulates elastin and collagen biosynthesis in vascular smooth muscle cells and skin fibroblasts by pretranslational mechanisms," *Journal of Biological Chemistry*, vol. 272, no. 1, pp. 345–352, 1997.

[94] S. R. Pinnell, "Regulation of collagen biosynthesis by ascorbic acid: a review," *Yale Journal of Biology and Medicine*, vol. 58, no. 6, pp. 553–559, 1985.

[95] E. Novoseletskaya, O. Grigorieva, P. Nimiritsky et al., "Mesenchymal stromal cell-produced components of extracellular matrix potentiate multipotent stem cell response to differentiation stimuli," *Frontiers in Cell and Developmental Biology*, vol. 8, Article ID 555378, 2020.

[96] C. Frantz, K. M. Stewart, and V. M. Weaver, "The extracellular matrix at a glance," *Journal of Cell Science*, vol. 123, no. 24, pp. 4195–4200, 2010.

[97] Y. Maehata, S. Takamizawa, S. Ozawa et al., "Type III collagen is essential for growth acceleration of human osteoblastic cells by ascorbic acid 2-phosphate, a long-acting vitamin C derivative," *Matrix Biology*, vol. 26, no. 5, pp. 371–381, 2007.

[98] D. Ulrich, I. Le Teuff, S. Huberlant, P. Carteron, V. Letouzey, and R. De Tayrac, "A preclinical evaluation of polypropylene/polylacticacid hybrid meshes for fascial defect repair using a rat abdominal hernia model," *PLoS One*, vol. 12, no. 6, Article ID e0179246, 2017.

[99] K. Stevenson, U. Kucich, C. Whitbeck, R. M. Levin, and P. S. Howard, "Functional changes in bladder tissue from type III collagen-deficient mice," *Molecular and Cellular Biochemistry*, vol. 283, no. 1-2, pp. 107–114, 2006.

[100] M. A. T. Bortolini, S. M. Feitosa, A. P. M. Bilhar et al., "Molecular and histomorphological evaluation of female rats' urethral tissues after an innovative trauma model of prolonged vaginal distention: immediate, short-term and long-term effects," *International Urogynecology Journal*, vol. 30, no. 3, pp. 465–476, 2019.

[101] C. M. Deveaud, E. J. Macarak, U. Kucich, D. H. Ewalt, W. R. Abrams, and P. S. Howard, "Molecular analysis of collagens in bladder fibrosis," *The Journal of Urology*, vol. 160, no. 4, pp. 1518–1527, 1998.

[102] L. S. Baskin, S. C. Constantinescu, P. S. Howard et al., "Biochemical characterization and quantitation of the collagenous components of urethral stricture tissue," *The Journal of Urology*, vol. 150, pp. 642–647, 1993.

[103] D. Zupančič, K. Mrak Poljšak, and M. E. Kreft, "Co-culturing porcine normal urothelial cells, urinary bladder fibroblasts and smooth muscle cells for tissue engineering research," *Cell Biology International*, vol. 42, no. 4, pp. 411–424, 2018.

[104] J. Liu, J. Huang, T. Lin, C. Zhang, and X. Yin, "Cell-to-cell contact induces human adipose tissue-derived stromal cells to differentiate into urothelium-like cells in vitro," *Biochemical and Biophysical Research Communications*, vol. 390, no. 3, pp. 931–936, 2009.

[105] W. R. Cross, I. Eardley, H. J. Leese, and J. Southgate, "A biomimetic tissue from cultured normal human urothelial cells: analysis of physiological function," *American Journal of Physiology - Renal Physiology*, vol. 289, no. 2, pp. 459–468, 2005.

[106] H. Fernandes, A. Mentink, R. Bank, R. Stoop, C. Van Blitterswijk, and J. De Boer, "Endogenous collagen influences differentiation of human multipotent

mesenchymal stromal cells," *Tissue Engineering Part A*, vol. 16, no. 5, pp. 1693–1702, 2010.

[107] Y. Saitoh, A. Morishita, S. Mito, T. Tsujiya, and N. Miwa, "Senescence-induced increases in intracellular oxidative stress and enhancement of the need for ascorbic acid in human fibroblasts," *Molecular and Cellular Biochemistry*, vol. 380, no. 1-2, pp. 129–141, 2013.

[108] B. Weiser, F. Sommer, M. Neubauer et al., "Ascorbic acid enhances adipogenesis of bone marrow-derived mesenchymal stromal cells," *Cells Tissues Organs*, vol. 189, no. 6, pp. 373–381, 2009.

[109] W. C. C. Lee, J. P. Rubin, and K. G. Marra, "Regulation of α-smooth muscle actin protein expression in adipose-derived stem cells," *Cells Tissues Organs*, vol. 183, no. 2, pp. 80–86, 2006.

[110] B. Piersma, O. Y. Wouters, S. de Rond, M. Boersema, R. A. F. Gjaltema, and R. A. Bank, "Ascorbic acid promotes a TGFβ1-induced myofibroblast phenotype switch," *Physiological Reports*, vol. 5, no. 17, Article ID e13324, 2017.

[111] B. Hinz, G. Celetta, J. J. Tomasek, G. Gabbiani, and C. Chaponnier, "Alpha-smooth muscle actin expression upregulates fibroblast contractile activity," *Molecular Biology of the Cell*, vol. 12, no. 9, pp. 2730–2741, 2001.

[112] A. Mykuliak, A. Yrjänäinen, A. J. Mäki et al., "Vasculogenic potency of bone marrow- and adipose tissue-derived mesenchymal stem/stromal cells results in differing vascular network phenotypes in a microfluidic chip," *Frontiers in Bioengineering and Biotechnology*, vol. 10, Article ID 764237, 2022.